UNIVERSITY OF BIRMINGHAM

Extragalactic Astrophysics and Cosmology
Cosmic Re-ionization

School of Physics and Astronomy
University of Birmingham

Joe Baumber, James Bryant, Lewis Clegg, Bethany Johnson, Andrew King,
Owen McConnell, Catherine McDonald, Michael O'Neill, Jonathan Shepley,
Dorothy Stonell, Rahim Topadar, Josh Wainwright

Supervisors: Graham Smith, Alistair Sanderson, Melissa Gillone

Date: March 2013

Abstract

This is a block of writing that is taking the place of the abstract. This is a block of writing that is taking the place of the abstract. This is a block of writing that is taking the place of the abstract. This is a block of writing that is taking the place of the abstract. This is a block of writing that is taking the place of the abstract. This is a block of writing that is taking the place of the abstract. This is a block of writing that is taking the place of the abstract. This is a block of writing that is taking the place of the abstract.

Contents

List of Figures

List of Tables

1   Introduction

The evolution of the Universe has been divided up by cosmologists into several epochs; each characterised by their unique physical properties. This project focuses on the Epoch of Re-ionization (EoR) whereby high energy photons produced during active star formation ionized the neutral hydrogen in the Inter-Galactic Medium (IGM). In order to probe this particular era and learn more about it, early (high redshift) galaxies are being studied as it is believed that they produced these first ionizing photons and hence their birth should understandably correlate directly to the beginning of the Epoch of Cosmic Re-ionization. This shall be discussed in more detail in Section **??**.

There are many unanswered questions in cosmology; one of the most crucial is the nature of dark energy and dark matter which make up around 95% of the universe [1]. These mysterious substances are thought to be the key driving force behind the evolution and expansion of the universe. By studying and mapping the distribution of Hydrogen during the EoR and tracking the evolution of stars and galaxies we are able to infer more about the effects of dark energy and what it might consist of. There are many different theories about what dark matter might consist of; the current most popular theories fall under the "Cold Dark Matter" model where dwarf galaxies are thought to be key building blocks in the hierarchical structure formation of the first galaxies [2].

The process of Cosmic Re-ionization is crucial to our understanding of the evolution of the Universe as it forms the bridge between our present and a distant, little-understood past. It links our current familiar universe, where stars and galaxies are more common than the grains of sand on Earth's beaches, to its past; when the Universe was a barren soup of free particles devoid of structure and life as we know it. Understanding the mechanisms of structure formation and what drives the collapse and formation of structure is fundamental in refining the Concordance Cosmology Model. Completing the picture of what happened during the EoR will enable us to more accurately predict where the Universe is headed and how it may eventually end, will it be in a "big crunch" or a "big freeze"?

The light from this era is so far away, and hence dim, that technology is only just allowing astronomers to see these early galaxies using high-powered telescopes and sophisticated detection processes. There are a number of different projects in progress investigating this particular period of the universe and there are many more in the pipeline, these will be discussed in more detail in part III.

1.1   Structure of Study

This study aims to develop an observing strategy based on original calculations for galaxy distributions and ultimately estimate the redshift range over which the EoR occurred. The group is split into two subgroups; a predictions group and an observational strategy group. The principal aim of the predictions group is to produce a set of calculations yielding the number of galaxies within the appropriate range of redshifts for re-ionization, with the inclusion of influences such as cosmic variance which skew the distribution. By considering the star formation rates and the ionization rate of neutral hydrogen the upper and lower bounds of this range respectively are determined. The final observing strategy explores which facilities to use; both current and planned and any adjustments required. The plan calculates the amount of observing time required to identify and confirm the properties of galaxies during the EoR. It also considers how to

limit objects which will spoil our results; contaminants such as foreground stars and Supernovae events. The strategy aims to see further than previously achieved in this field and help to drive the understanding of re-ionization to new heights.

Part I
General Theory

Part II

Predictions

Part III

Observations

2 Spectroscopy

The spectrum of typical high redshift galaxy can be seen in Figure 1.
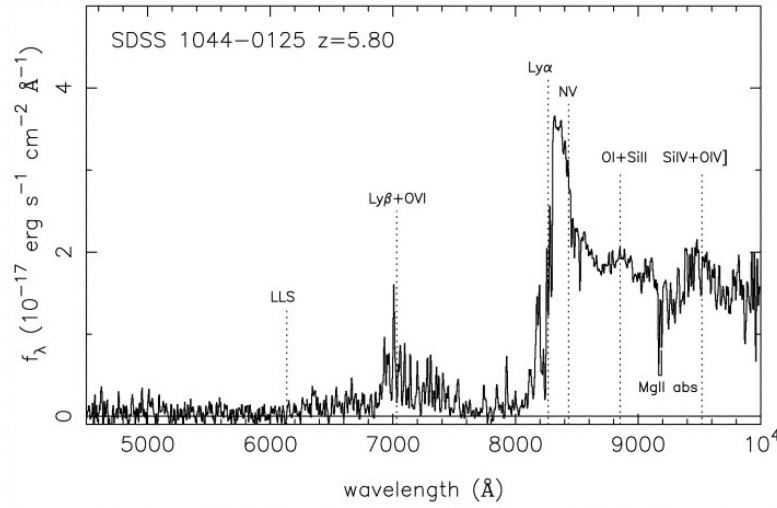

Figure 1

The distinct drop in emission is due to the presence of neutral hydrogen around the galaxies, known as the Gunn Peterson trough. Therefore the galaxies where formed before the start of re-ionisation. This is discussed in detail in Section **??**. However this particular feature in the spectra is of great importance here. The wavelength at which this drop occurs corresponds to the amount of energy required for an electron to transition between the first two energy levels in neutral hydrogen. This is known as the Lyman-α transition line and has a rest frame wavelength here on earth of 1216 Å [][1][2]. However, the actual wavelength that this drop occurs in the spectrum of the galaxy being studied will be much longer. In Figure 1, it is closer to 8000 Å. This is due to the fact that the light is red shifted effectively stretching the wavelength. Indeed, the observed wavelength of the Lyman-α transition line will be in the infrared range. If this wavelength can be measured precisely then the redshift of the galaxy can be calculated [][2]. This is done using the relation,

$$1 + z = \frac{\lambda_{\text{observed}}}{\lambda_{\text{emitted}}} \tag{2.1}$$

Hence, spectroscopy can be used to confirm the high-red shift galaxy candidates that are identified via photometry. In essence it is high resolution photometry.

An astronomical spectrograph splits or disperses light from a source into its constituent wavelengths. Therefore it has to have some means of dispersing the light. The simplest way this can

be achieved is via a prism. This exploits the fact that different wavelengths are diffracted via different amounts. However, they are rarely used by themselves in astronomical spectroscopy due to their inefficiency. Only about 10% of the light incident upon them actually gets dispersed. Moreover, the dispersion is nonlinear causing some light to be dispersed more than others. Therefore, the universal dispersing medium used in astronomical spectroscopy is the diffraction grating. A diffraction grating consists of a large number of equidistant parallel lines ruled onto a transparent glass plate. The incident light cannot travel through the grating, but is instead channelled along the parallel lines. As the light reaches the end of the lines it is diffracted producing a series of wavelets in accordance with Huygens's Principle. These either constructively or destructively interfere producing a series of maxima or minima. Again, different wavelengths of light will be diffracted through different angles. Therefore each maximum (order) can be thought of as the image of the galaxy split into its constituent wavelengths. As a general rule, the first maximum is projected onto the CCD equipment of the telescope and used to calculate the redshift. This is due to the fact it has the highest intensity. Figures 2 and 3 below show a schematic of a grating being used to split light
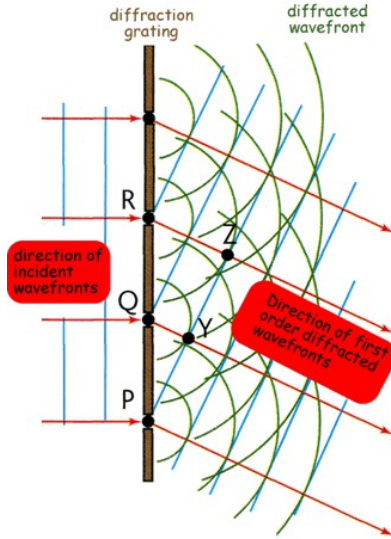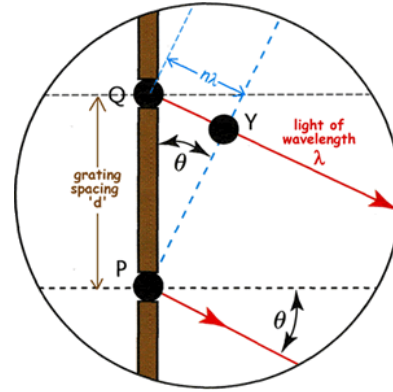

Figure 2

Figure 3

Angles at which the orders occur can be found using the grating equation,

$$n\lambda = d(\sin\theta + \sin\phi) \tag{2.2}$$

Where ϕ is the angle of incidence between the light and the grating, θ is the angle of dispersion and d is the grating spacing. The value of $n\lambda$ is an integer number of wavelengths of the incident light.

Before light reaches either a prism or diffraction grating it is often sent through a fixed slit. This is a mask with a narrow rectangular aperture that is placed in the focal plane of the telescope. The slit has two main functions. First and foremost it isolates a portion of the sky of interest so that only light that falls on the slit may enter the spectrograph. This is important as it means the spectra from different parts of a galaxy cannot enter the spectrograph, overlap and thus contaminate each other. Second, the slit provides a stable spectral resolution. Without the slit

the spectral resolution would be defined by the width of the galaxy or star. However, this varies with time so the spectral line width would vary with time. This would make detailed analysis of the spectrum almost impossible. If on the other hand a slit is used, the spectrum becomes an infinite number of images of the slit, and not the galaxy or star etc. As the slit width is constant, the spectral resolution remains stable.

In between the slit and dispersion medium usually sits a collimator. The light from the slit diverges and if left would hit the grating or prism at differing angles of incidence making the resulting spectrum useless. Therefore a collimator is used to turn the diverging light back to parallel. Figure 4 below shows the set-up for NIRspec on the JWST.
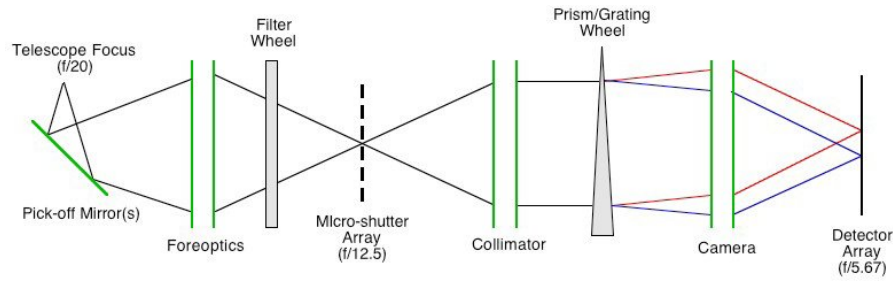

Figure 4

2.1 Candidate Telescopes

2.1.1 James Webb Space Telescope

The primary telescopes considered for use in this research are the JWST and the E-ELT. The JWST's NIRSpec is a device which will enable the conformation of high red shift galaxies. It uses a combination of slits, prims and gratings to achieve high resolution spectroscopy. Perhaps its most innovative feature is a microshutter array. The microshutters are tiny cells that measure $100 \times 200\,\mu$m. They are arranged over a waffle like grid containing $62\,000$ individual cells. NIRSpec will contain four identical grids in total. The cells all have lids which can be opened and closed individually. This is achieved by sweeping a magnet across the surface of the array which opens all of the lids and the electronically closing individual lids. Each cell measures 203×463 milliarcseconds. The total field of view for all four arrays combined is 3×3 arcminutes. Shutters in each array can be opened or closed to form multiple apertures meaning that spectrums for one hundred different targets can be found simultaneously. The size and shape of the apertures can be selected to obtain the clearest spectrum possible for each individual target. Figures 5 and 6 show NIRSpec under construction [][7] [][8].

As well as the microshutter array the JWST also contains an integral field unit. Integral field spectroscopy has become an important sub discipline of astronomy where there is a need to study the spectra of extended bodies. This has particular significance as high red shift galaxies are considered to be extended bodies.

Integral field spectroscopy is the successor to long slit spectroscopy where the spectrum is dispersed perpendicular to the slit direction. By stepping the position of the slit the spectrum of points over the extended body can be obtained. An integral field unit speeds up this process
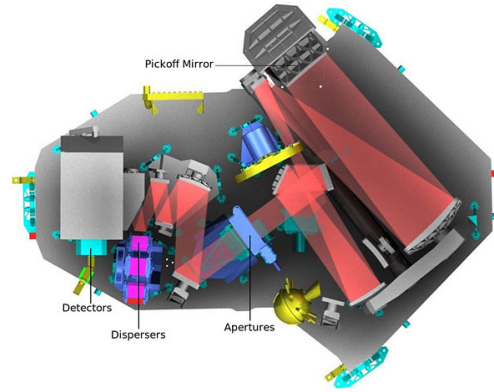
Figure 5

Figure 6

by slicing the image and then rearranging it so that different parts can illuminate the slit. This negates the need to take multiple exposures [][9] [][10].

NIRSpec will be able to disperse light comprised of wavelengths between 0.6 and 5 microns, i.e. the infrared range over which the Gunn Peterson trough should occur. It will do this using one prism and five diffraction gratings. The wavelength ranges over which each will work and their associated wavelengths are shown below [][11].

Grating	Filter	Resolution	Wavelength (µm)
Prism	Clear	100	0.5–5
G140M	F100LP	1000	1.0–1.8
G235M	F170LP	1000	1.7–3.0
G395M	F290LP	1000	2.9–5.0
G140M	F100LP	2700	1.0–1.8
G235M	F170LP	2700	1.7–3.0
G395M	F290LP	2700	2.9–5.0

Table 1: *Number of galaxies for set total observing time given different magnitudes/ survey areas for JWST.*

2.2 European Extremely Large Telescope

The European-Extremely Large Telescope (E-ELT) will be equipped with three spectroscopic devices:

1. EAGLE - A multichannel integral field near infrared spectrograph with multi object adaptive optics;

2. HARMONI - A wide band field spectrograph;

3. SIMPLE – Echelle high resolution spectrograph.

EAGLE will enable spectrums of multiple galaxies to be obtained simultaneously and thus would be of great benefit for this project. However, as it is only in early development stage information

required to perform estimates for exposure times is not available. It is most likely to use a system of fibre optics to stack spectrums of galaxies onto the CCD. The fibre optics will sit between the diffraction grating and the CCD. As mentioned above it will use a system of multi object adaptive objects. This will use separate pieces of a deformable mirror to compensate for distortions across all the objects in its field of view. The correction applied to these mirrors will be determined by atmospheric tomography using guide stars [][12].

SIMPLE uses an echelle grating in order to achieve resolving powers up to 130 000. It will work over a wavelength range of 0.8–2.5µm. In order to understand how echelle gratings can achieve such high resolution we must first consider blazing. The fact that diffraction gratings produce multiple spectra of the same object means that they are very inefficient. Most of the light incident upon a grating will fall in the zeroth order which is undispersed. Only about 10% of the light will be contained within the first order; the higher the order, the less the percentage. To change these proportions the prism must be blazed. This involves tilting the surface of the grooves by some angle known as the blazing angle. This angle is such that a light ray will emerge from the grating as if by reflection. It is therefore possible to direct as much as 70% of the light in the order of interest. Without exception the spectrum of different orders will overlap causing contamination. The higher the order, the worse the contamination as the angle through which the spectrum is dispersed is greater. However, for this very reason resolution is much improved. Echelle gratings are therefore blazed in such a way that most of the light falls anywhere from the 10th to the 100th order depending on the blazing angle. In order to remove the contamination present at such orders echelle gratings are used in tandem with cross dispersers. These are low dispersion gratings or prisms with a dispersion axis perpendicular to that of the echelle grating. Their function is to separate out the overlap, thus providing an extremely high resolution spectrum [][13] [][14].

HARMONI is a visible and near infrared integral field spectrograph with a field of view of 5×10 arc minutes. It will cover a wavelength range of 0.47 to 2.45 µm and enable resolving powers from 4000 to 20 000 providing the E-ELT's core spectroscopic capability. HARMONI provides a range of spatial pixel scales which enable the user to configure the instrument of a multitude of science goals. It can adapt to any flavour of adaptive optics and therefore negate any distortions in light from distant galaxies caused by Earth's atmosphere **??**(See Rahiims section on adaptive optics). The wavelength ranges of the diffraction gratings can be seen in the table below [][15] [][16].

Band/Grating	Resolution	Wavelength (µm)
H+K	3900	1.4-2.4
I+Z+J	3857	0.8-1.4
K	8800	2.0-2.5
H	8892	1.5-1.8
J	8714	1.1-1.4
I+Z	8809	0.8-1.0
K	High	19174 2.1-2.3
H	High	19176 1.5-1.7
J	High	20500 1.2-1.3
z	19222	0.8-0.9

Table 2: *Number of galaxies for set total observing time given different magnitudes/ survey areas for JWST.*

2.3 Calculation of Exposure Times

The method of calculation for spectroscopic exposure times is much the same as for photometry discussed previously. However, light from the galaxies will not fall in one place on the CCD; instead it will be dispersed by the grating or prism in the spectrometer device. Therefore, it is not possible to use the same equation to determine N_{pix} as has been done previously. In order to calculate N_{pix} for spectroscopy, the spectral resolution of the dispersive medium being used must first be considered. This can be found using the relationship

$$R = \frac{\lambda}{\Delta\lambda} \tag{2.3}$$

Where R is the resolving power of the diffraction grating or prism and λ is the red-shifted wavelength of the Lyman-α absorption line. If these are both known then, $\Delta\lambda$ the spectral resolution can be found for the diffraction grating or prism being used. This is put in place of the band width used in photometry. Light will fall on the CCD in a narrow strip across its width. For the purposes of simplicity, this report will assume that light falls across the entire width of the CCD. The wavelength range this corresponds to is just the wavelength range that can be dispersed particular to the grating or prism being used. The number of pixels across the width of the CCD is known, therefore the wavelength range to which each pixel corresponds can be found. Hence, the number of pixels the spectral resolution can also be found. This value is then multiplied by the spatial resolution element, the number of pixels on the CCD to which the galaxy subtends, to give N_{pix}. The spatial resolution element has been found to be in the order of a few for the size and redshifts of galaxies considered [][17].

Background for the JWST will mainly be from zodiacal light and thermal radiation from the sun. However, like the flux from the galaxies being observed it will be dispersed by the prism or grating in the spectrometer. Therefore, to calculate the total sky background, the background per pixel is multiplied by the number of pixels in each spectral resolution element.

In order to estimate the exposure times more accurately the width the spectrums cover the CCD must be known. For a given distance between the dispersive medium and CCD this can be found, but as the spectroscopic devices for the JWST and E-ELT are still undergoing development this distance is unknown. When using NIRSpec's multi-shutter array for multi-object spectroscopy, the widths of the spectrums will depend where the galaxies fall within the field of view, and will not necessarily fit across the entire width of the CCD. This is shown below...

However, both the JWST and the E-ELT have been designed to optimise the space on the CCD to achieve a maximum resolution. The estimates of exposure times will be upper limits as the calculations are integrated over the maximum number of pixels possible by using the full width of the CCD.

A method for more accurate calculation of exposure times is given below providing all relevant information regarding the spectrographs is known, it is a slight variation on the method used for photometry

$$C = \frac{I_\lambda N_{\lambda\text{spix}} S_\lambda^d N_{\lambda\text{spix}}}{G} \tag{2.4}$$

where

- C = Counts per pixel from astronomical source,
- S = Instrument spectral sensitivity,

- G = Gain (This is the conversion from electrons to ADUs),

- I = Flux from the astronomical source,

- $N_{\lambda\text{spix}}$ = Number of pixels in the spatial direction,

- $N_{\lambda\text{spix}}$ = Number of pixels in the spectral direction.

Having found the Counts we can then use equation (below) to find the time required for a desired signal to noise ratio

$$\frac{S}{N} = \frac{CtG}{\sqrt{CtG + N_{\text{pix}}(B_{\text{sky}} + B_{\text{det}})Gt + \frac{N_{\text{pix}}}{N_{\text{bin}}}(N_{\text{read}}R^2)}} \tag{2.5}$$

where

- t = Exposure time (s),

- N_{pix} = Number of pixels integrated over,

- B_{sky} = Sky background (photons/sec/pixel),

- N_{bin} = Total number of binned pixels on CCD,

- N_{read} = Number of CCD readouts,

- R = Read noise (electrons) [][18] [][19].

References

[1] G. Hinshaw, D. Larson, E. Komatsu, D. N. Spergel, C. L. Bennett, J. Dunkley, M. R. Nolta, M. Halpern, R. S. Hill, N. Odegard, L. Page, K. M. Smith, J. L. Weiland, B. Gold, N. Jarosik, A. Kogut, M. Limon, S. S. Meyer, G. S. Tucker, E. Wollack, and E. L. Wright. Nine-Year Wilkinson Microwave Anisotropy Probe (WMAP) Observations: Cosmological Parameter Results. *ArXiv e-prints*, December 2012.

[2] M. Cignoni and M. Tosi. Star Formation Histories of Dwarf Galaxies from the Colour-Magnitude Diagrams of Their Resolved Stellar Populations. *Advances in Astronomy*, 2010, 2010.

[3] N. A. Reddy and C. C. Steidel. A Steep Faint-End Slope of the UV Luminosity Function at z ~ 2-3: Implications for the Global Stellar Mass Density and Star Formation in Low-Mass Halos. *apj*, 692:778–803, February 2009.

[4] R. J. McLure, J. S. Dunlop, M. Cirasuolo, A. M. Koekemoer, E. Sabbi, D. P. Stark, T. A. Targett, and R. S. Ellis. Galaxies at z = 6-9 from the WFC3/IR imaging of the Hubble Ultra Deep Field. *mnras*, 403:960–983, April 2010.

[5] R. J. Bouwens, G. D. Illingworth, M. Franx, and H. Ford. UV Luminosity Functions at z~4, 5, and 6 from the Hubble Ultra Deep Field and Other Deep Hubble Space Telescope ACS Fields: Evolution and Star Formation History. *apj*, 670:928–958, December 2007.

[6] R. J. Bouwens, G. D. Illingworth, P. A. Oesch, I. Labbé, M. Trenti, P. van Dokkum, M. Franx, M. Stiavelli, C. M. Carollo, D. Magee, and V. Gonzalez. Ultraviolet Luminosity Functions from 132 z ~ 7 and z ~ 8 Lyman-break Galaxies in the Ultra-deep HUDF09 and Wide-area Early Release Science WFC3/IR Observations. *apj*, 737:90, August 2011.

A Derivation of Thermal Background

Number of incident photons, N_γ, is

$$N_\gamma = \int_{\nu_1}^{\nu_2} \frac{\epsilon B_\nu(T)}{h\nu}\, \mathrm{d}\nu \tag{A.1}$$

This integral spans the filter from the red to the blue end, where ν is the frequency of light, h is Planck's constant and B_ν is given by:

$$B_\nu(T) = \frac{2h\nu^3}{c^2} \frac{1}{\mathrm{e}^{\frac{h\nu}{kT}} - 1} \tag{A.2}$$

where c is the speed of light, T is the temperature of, k is Boltzmann's constant and $\mathrm{e}^{\frac{h\nu}{kT}} \ll 1$. Using the substitution

$$x = \frac{h\nu}{kT}, \qquad \nu = \frac{kTx}{h} \tag{A.3}$$

$$\Rightarrow \mathrm{d}\nu = \frac{kT}{h}\, \mathrm{d}x \tag{A.4}$$

$B_\nu(T)$, then, is

$$B_\nu(T) = \frac{2k^3 T^3 x^3}{h^2 c^2} \frac{1}{\mathrm{e}^x} \tag{A.5}$$

Thus, the number of photons is given by

$$N_\gamma = \frac{2k^3 T^3 \epsilon}{h^2 c^2} \int_{x_1}^{x_2} x^2 \mathrm{e}^{-x}\, \mathrm{d}x \tag{A.6}$$

$$= \frac{2k^3 T^3 \epsilon}{h^2 c^2} \left[-x^2 \mathrm{e}^{-x} + \int \mathrm{e}^{-x} \cdot 2x\, \mathrm{d}x \right]_{x_1}^{x_2} \tag{A.7}$$

$$= \frac{2k^3 T^3 \epsilon}{h^2 c^2} \left[-x^2 \mathrm{e}^{-x} - 2x\mathrm{e}^{-x} + \int 2\mathrm{e}^{-x}\, \mathrm{d}x \right]_{x_1}^{x_2} \tag{A.8}$$

$$= \frac{2k^3 T^3 \epsilon}{h^2 c^2} \left[-\mathrm{e}^{-x}\left(x^2 + 2x + 2\right) \right]_{x_1}^{x_2} \tag{A.9}$$

By integrating from the blue end of the filter to the red, we can remove the negative sign to give

$$N_\gamma = \frac{2k^3 T^3 \epsilon}{h^2 c^2} \left[\mathrm{e}^{-x}\left(x^2 + 2x + 2\right) \right]_{x_1}^{x_2} \tag{A.10}$$

B Parameter Fit Data

B.1 Faint End Slope Data

B.2 Normalisation Data

B.3 Characteristic Magnitude Data

Rest λ (Å)	z	error z	α	pos error ϕ^*	neg error ϕ^*	upper z	lower z	upper	lower	Citation
1750	8		-1.91	0.32	0.09	8	8	-2	-1.59	[]
1750	8		-1.67	0.4	0.4	8	8	-2.07	-1.27	[]
1700	2.3	0.4	-1.73	0.07	0.07	2.7	1.9	-1.8	-1.66	[]
1700	3.05	0.35	-1.73	0.13	0.13	3.4	2.7	-1.86	-1.6	[]
1500	7	0.5	-1.72	0	0	7.5	6.5	-1.72	-1.72	[]
1500	5	0.3	-1.66	0.06	0.06	5.3	4.7	-1.72	-1.6	[]
1500	6	0.3	-1.71	0.11	0.11	6.3	5.7	-1.82	-1.6	[]
1600	3.8		-1.76	0.05	0.05	3.8	3.8	-1.81	-1.71	[]
1600	5		-1.69	0.09	0.09	5	5	-1.78	-1.6	[]
1600	6.8		-1.895	0.1045	0	6.8	6.8	-1.895	-1.791	[]
1600	3.8		-1.73	0.05	0.05	3.8	3.8	-1.78	-1.68	[]
1600	5		-1.66	0.09	0.09	5	5	-1.75	-1.57	[]
1350	5.9		-1.74	0.16	0.16	5.9	5.9	-1.9	-1.58	[]
1350	5.9		-1.77	0.16	0.16	5.9	5.9	-1.93	-1.61	[]

Table 3: *Data describing the evolution of the faint end slope parameter, α.*

Rest λ (Å)	z	error z	ϕ^*	pos error ϕ^*	neg error ϕ^*	upper z	lower z	upper	lower	Citation
1750	8		5.90E-04	1.01E-03	3.70E-04	8	8	1.60E-03	2.20E-04	[]
1750	8		1.50E-03	2.90E-03	1.00E-03	8	8	4.40E-03	5.00E-04	[]
1700	2.3	0.4	2.75E-03	5.40E-04	5.40E-04	2.7	1.9	3.29E-03	2.21E-03	[]
1700	3.0	0.35	1.71E-03	5.30E-04	5.30E-04	3.4	2.7	2.24E-03	1.18E-03	[]
1500	7	0.5	7.00E-04	0	0	7.5	6.5	7.00E-04	7.00E-04	[]
1500	5	0.3	9.00E-04	2.00E-04	2.00E-04	5.3	4.7	1.10E-03	7.00E-04	[]
1500	6	0.3	1.80E-03	0	0	6.3	5.7	1.80E-03	1.80E-03	[]
1600	3.8		1.10E-03	2.00E-04	2.00E-04	3.8	3.8	1.30E-03	9.00E-04	[]
1600	5		9.00E-04	3.00E-04	2.00E-04	5	5	1.20E-03	7.00E-04	[]
1600	6.8		8.60E-04	7.00E-04	3.90E-04	6.8	6.8	1.56E-03	4.70E-04	[]
1600	3.8		1.30E-03	2.00E-04	3.00E-04	3.8	3.8	1.50E-03	1.00E-03	[]
1600	5		1.00E-03	3.00E-04	3.00E-04	5	5	1.30E-03	7.00E-04	[]
1350	5.9		1.50E-03	2.90E-03	1.00E-03	5.9	5.9	4.40E-03	5.00E-04	[]
1350	5.9		1.40E-03	6.00E-04	4.00E-04	5.9	5.9	2.00E-03	1.00E-03	[]

Table 4: *Data describing the evolution of the Schechter normalisation parameter, ϕ^*.*

Rest λ (Å)	z	error z	M^*	error M^*	upper z	lower z	upper	lower	Citation
1750	8		-20.1	0.52	8	8	-20.62	-20.1	[3]
1750	8		-19.54	0.56	8	8	-20.1	-19.54	[3]
1700	2.3	0.4	-20.7	0.11	2.7	1.9	-20.81	-20.7	[3]
1700	3.05	0.35	-20.97	0.14	3.4	2.7	-21.11	-20.97	[3]
1500	7	0.5	-20.11		7.5	6.5	-20.11	-20.11	[4]
1500	5	0.3	-20.73	0.11	5.3	4.7	-20.84	-20.73	[4]
1500	6	0.3	-20.04	0.12	6.3	5.7	-20.16	-20.04	[4]
1600	3.8		-21.06	0.1	3.8	3.8	-21.16	-21.06	[5]
1600	5		-20.69	0.13	5	5	-20.82	-20.69	[5]
1600	6.8		-20.14	0.26	6.8	6.8	-20.4	-20.14	[6]
1600	3.8		-20.98	0.1	3.8	3.8	-21.08	-20.98	[6]
1600	5		-20.64	0.13	5	5	-20.77	-20.64	[6]
1350	5.9		-20.24	0.19	5.9	5.9	-20.43	-20.24	[6]
1350	5.9		-20.29	0.19	5.9	5.9	-20.48	-20.29	[5]

Table 5: *Data describing the evolution of the charachteristic magnitude parameter, M^*.*